ACS APPLIED MATERIALS & INTERFACES

Research Article

www.acsami.org

Solvothermal Synthesis of Monodisperse $LiFePO_4$ Micro Hollow Spheres as High Performance Cathode Material for Lithium Ion Batteries

Shiliu Yang, Mingjun Hu, Liujiang Xi, Ruguang Ma, Yucheng Dong, and C. Y. Chung*

Department of Physics and Materials Science, City University of Hong Kong, 83 Tat Chee Avenue, Kowloon Tong, Hong Kong, P. R. China

Supporting Information

ABSTRACT: A microspherical, hollow $LiFePO_4$ (LFP) cathode material with polycrystal structure was simply synthesized by a solvothermal method using spherical Li_3PO_4 as the self-sacrificed template and $FeCl_2{\cdot}4H_2O$ as the Fe^{2+} source. Scanning electron microscopy (SEM) and transmission electron microscopy (TEM) show that the LFP micro hollow spheres have a quite uniform size of ~1 μm consisting of aggregated nanoparticles. The influences of solvent and Fe^{2+} source on the phase and morphology of the final product were chiefly investigated, and a direct ion exchange reaction between spherical Li_3PO_4 templates and Fe^{2+} ions was firstly proposed on the basis of the X-ray powder diffraction (XRD) transformation of the products. The LFP nanoparticles in the micro hollow spheres could finely coat a uniform carbon layer ~3.5 nm by a glucose solution impregnating−drying−sintering process. The electrochemical measurements show that the carbon coated LFP materials could exhibit high charge−discharge capacities of 158, 144, 125, 101, and even 72 mAh g^{-1} at 0.1, 1, 5, 20, and 50 C, respectively. It could also maintain 80% of the initial discharge capacity after cycling for 2000 times at 20 C.

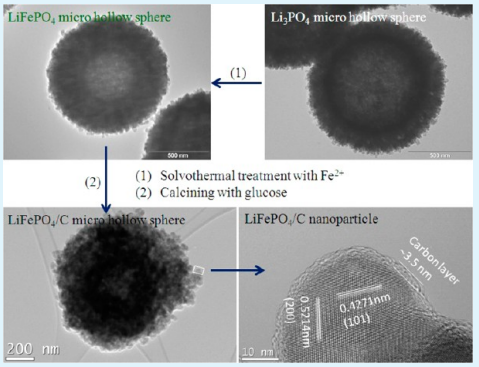

KEYWORDS: *$LiFePO_4$, Li_3PO_4, solvothermal, ion exchange, micro hollow spheres, lithium ion batteries*

1. INTRODUCTION

As one of the most promising cathode materials for future electric vehicles (EVs), plug-in hybrid EVs, and energy storage,[1−4] $LiFePO_4$ (LFP) has attracted vast attention all over the world since it was reported in 1997,[5−14] owing to the virtues of low cost and environmentally benign and good thermal stability plus the characteristics of high reversible theoretical capacity (170 mAh g^{-1}) and perfect flat voltage profile at 3.45 V vs Li^+/Li as compared with other cathode materials currently used in commercial lithium ion batteries.[15,16] However, the LFP suffers from two main disadvantages such as low ionic−electronic conductivity (10^{-9}−10^{-10} S cm^{-1}) and limited lithium ion diffusion channel (one-dimensional path along the *b*-axis of the olivine-structured LFP),[17−19] which limit its commercial use. During the past decade, tremendous efforts have been focused on overcoming the kinetic limitation of the LFP materials through particle-size minimization accompanied by external conductive coating and internal cationic doping.[2,6,10,20−30] Nevertheless, nanomaterials usually have high surface area leading to undesirable electrode/electrolyte reactions and inferior packing of particles leading to some problems on the electrode preparation.[3] In order to solve these problems without consuming the electrochemical performances, synthesis of carbon coated LFP materials with mesoporous solid or hollow spherical morphology was strongly suggested in recent years.[31−39]

Up to now, there are several chief methods to synthesize mesoporous solid LFP spheres. (i) Spray pyrolysis method: which is a simple and scalable method using aqueous or sol−gel precursors as the raw materials, but the spherical LFP materials synthesized by this method usually have a large size, over 10 μm;[40−43] the best result that could deliver a discharge capacity of 106 mAh g^{-1} at 20 C was claimed by Liu et al.[44] (ii) Solid state method: in which the micro porous spherical $MPO_4{\cdot}xH_2O$ (M = Fe or Mn−Fe) precursors were sintered with lithium sources to produce the microspherical LFP materials, and most of the LFP products also have a large size, over 5 μm.[27,45−50] The LFP microspheres with smaller size of 2 μm were reported to have a discharge capacity of 96 mAh g^{-1} at 20 C by Lou et al.[51] (iii) Hydrothermal or solvothermal methods:[52−59] which can synthesize many spherical LFP products with hierarchical structures and vast size distribution from 1 to 30 μm, and the micro porous LFP spheres prepared by Qian et al.[60] showed the best discharge capacity of 93 mAh g^{-1} at 20 C.

The microspherical hollow LFP materials were seldom reported by Lee et al.[61] and Huang et al.[62] who have prepared hierarchical LFP micro hollow spheres by using KIT-6 silica

Received: May 24, 2013
Accepted: August 27, 2013
Published: August 27, 2013

   dx.doi.org/10.1021/am401990b | ACS Appl. Mater. Interfaces 2013, 5, 8961−8967

and carbon spheres as the hard templates, respectively. These LFP materials can present superior discharge capacities of 153 mAh g^{-1} at 15 C and 101.5 mAh g^{-1} at 20 C, respectively. However, the hard template methods are time consuming and costly because of the need for the initial synthesis and the final removal of the template. Recently, Lee et al.[63] synthesized aggregated LFP sub-micro hollow spheres by a one-pot hydrothermal method and a subsequent sintering process using Li_3PO_4 as the precursor, which provided an interesting strategy to prepare the hollow structured LFP materials. Through controlling the precipitation processes and reaction conditions, LFP materials with different size and morphology were also studied by his group.[64,65]

In this paper, a monodisperse, microspherical, hollow Li_3PO_4 material with size distribution of ~1 μm was also used as the self-sacrifice template to synthesize LFP material by a simple solvothermal method using $FeCl_2{\cdot}4H_2O$ as the Fe^{2+} source in EG (ethylene glycol) medium. The influences of solvent and Fe^{2+} source on the phase and morphology of the final product were chiefly investigated, and a direct ion exchange reaction between spherical Li_3PO_4 templates and Fe^{2+} ions in EG was proposed. The nanoparticles in LFP micro hollow spheres could finely coat a uniform carbon layer ~3.5 nm by a glucose solution impregnating–drying–sintering process, and the carbon coated LFP could exhibit superior rate and cycling performances.

2. EXPERIMENTAL SECTION

2.1. Synthesis. All chemicals are analytical grade and used without further purification. The Li_3PO_4 spherical templates were firstly synthesized by a modified method reported in our previous paper.[66] In a typical procedure, a binary solvent of 5 mL of PEG600 (polyethylene glycol 600) and 15 mL of H_2O, which contains 4 mmol of H_3PO_4, was quickly poured into another identical binary solvent containing 12 mmol of LiOH under mild magnetic stirring at room temperature. A white suspension was formed and was further stirred for 15 min; then, the Li_3PO_4 product was collected by filtration and water–ethanol washing for several times. The final product was dried at 100 °C over 3 h. A typical synthesis procedure for LFP micro hollow spheres is below; 2 mmol of $FeCl_2{\cdot}4H_2O$ was dissolved into 5 mL of ethylene glycol (EG) solvent in an autoclave container. Then, 2 mmol of as-prepared Li_3PO_4 product was re-dispersed into the above solution by stirring for 15 min. The autoclave was filled with argon gas, sealed, and put into a preset electronic furnace for 3 h at 180 °C. After the reaction, the solution was filtrated, washed by water and ethanol, respectively, and dried in a vacuum at 80 °C for 3 h. Carbon coated LFP micro hollow spheres were achieved by a glucose solution impregnating–drying–sintering procedure. LFP product (0.1 g) was put into 250 μL of 0.1 M glucose solution; the slurry was magnetically stirred and dried at room temperature naturally, and then, the dried powder was sintered at 600 °C for 3 h under 5 vol % H_2/Ar atmosphere with a heating rate of 5 °C min^{-1}.

2.2. Characterization. X-ray powder diffraction (XRD) patterns of the products were obtained on a Philip X-ray diffractometer equipped with Cu Kα radiation (λ = 1.5405 Å) employing a scanning rate of 0.02° s^{-1} in the 2θ range from 10° to 50° with step time of 3 s. The scanning electron microscopy (SEM) images were taken on a field emission scanning electron microscope (Joel JSM-820, 15 kV, Hitachi, Japan). Transmission electron microscopy (TEM) and high resolution transmission electron microscopy (HRTEM) were carried out on a Hitachi H-800 transmission electron microscope and a JEOL JEM-2100F TEM/STEM operated at 200 kV, respectively. Thermogravimetric analysis (TGA) was carried out on a TGA Q5000 analyzer (TA Instruments) with a heating rate of 10 °C min^{-1} in a nitrogen or oxygen atmosphere.

2.3. Electrochemical Measurements. The composite electrode used for electrochemical measurements was prepared by grinding carbon coated LFP material, Super P carbon, and PVDF (polyvinyldifluoride) with the mass ratio of 7:2:1 in NMP (*N*-methylpyrrolidone). The slurry was spread onto an aluminum foil and dried at 100 °C for 3 h under vacuum condition. The circular cathode disc with diameter of 1.5 cm was punched from the aluminum foil, and the areal density of the active material (LFP excluding carbon content) was around 2 mg cm^{-2}. The coin type cells (size 2032) were assembled in an argon-filled glove box using Li metal as the anode, Celgard 2500 membrane as the separator, and 1M $LiPF_6$ solution in EC/DMC (ethylene carbonate/dimethyl carbonate, 1:1 by volume) as the electrolyte. Galvanostatic charging–discharging performances were evaluated with a model BT 200 battery cycler (Arbin Instruments, USA) at room temperature between 2 and 4.2 V for different current density (1 C rate corresponds to the current density of 170 mA g^{-1}). Cyclic voltammetry (CV) and electrochemical impedance spectroscopy (EIS) were analysed by a Zahner IM6 electrochemical station; the amplitude of the AC signal was 5 mV over the frequency range between 100 kHz and 0.01 Hz.

3. RESULTS AND DISCUSSION

3.1. Phase and Morphology Characterization of Li_3PO_4 and LFP. Figure 1a is the XRD pattern of the as-prepared Li_3PO_4 templates which can be clearly indexed to orthorhombic Li_3PO_4 (JCPDS No. 25-1030). The SEM image shows that the well dispersed Li_3PO_4 microspheres have a quite uniform size of 1 μm (Figure 2a). The TEM image indicates that the Li_3PO_4 microspheres exhibit interesting hollow or double hollow structures which may be caused by the sequential precipitation reaction of H_3PO_4 and LiOH (Figure 2b). The magnified TEM image and corresponding electron diffraction pattern show that the Li_3PO_4 micro hollow sphere is a polycrystal composed of aggregated nanoparticles (Figure 2c). The average sizes of the aggregated Li_3PO_4 nanoparticles were estimated as ~60 nm from the strongest detected (020) peak at 2θ value of 34.09° by using Scherrer's formula ($D = K\lambda/\beta\cos\theta$), where D was the particle size (nm), K was the Scherrer constant (0.89), λ was the wave length of the Cu Kα radiation

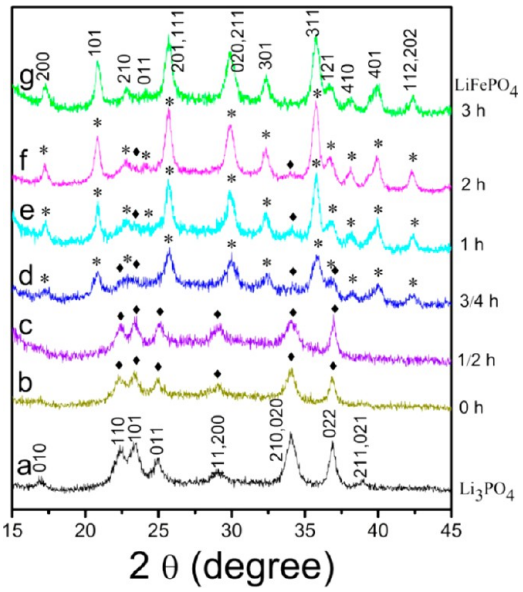

Figure 1. XRD patterns show the phase transformation from Li_3PO_4 to LFP. (a) As-prepared Li_3PO_4 micro hollow spheres; (b) to (g) were the samples collected after solvothermal treatment at 180 °C for different times: (b) 0 h, (c) 1/2 h, (d) 3/4 h, (e) 1 h, (f) 2 h, and (g) 3 h. [♦] Li_3PO_4, [*] LFP.

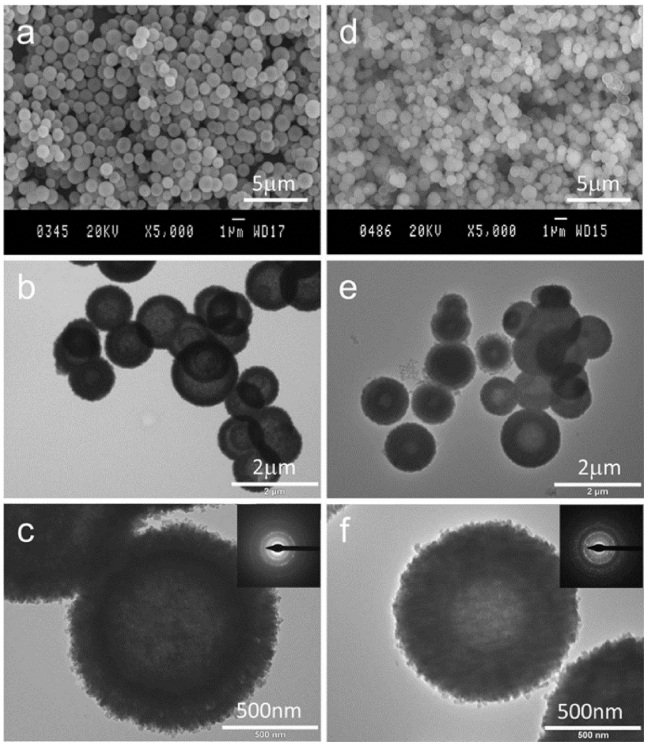

Figure 2. SEM and TEM images of the as-prepared Li_3PO_4 micro hollow spheres (a, b, c) and the as-prepared LFP micro hollow spheres (d, e, f). Inset is the electron diffraction patterns of Li_3PO_4 and LFP, respectively.

(0.15405 nm), β was the full width at half maximum (rad), and θ was the diffraction angle (degree).

The phase transformation from Li_3PO_4 to pure LFP was carefully investigated by the XRD patterns of the samples collected after different reaction times at 180 °C. When the Li_3PO_4 micro hollow spheres were dispersed into $FeCl_2{\cdot}4H_2O$/EG solution and stirred at room temperature for 15 min (i.e., 0 h at 180 °C), the XRD pattern shows no reaction between Li_3PO_4 and Fe^{2+} ions but a subtle decrease of the peak intensity of Li_3PO_4, which may be caused by the adsorption of the Fe^{2+} ions onto the surface of the Li_3PO_4 nanoparticles (Figure 1b). At the early stage of reaction of about 30 min at 180 °C, there was still no obvious reaction between Li_3PO_4 and Fe^{2+} ions (Figure 1c). However, after 45 min, the reaction between the Fe^{2+} ions and Li_3PO_4 occurred, and the XRD pattern shows a main phase of LFP with some unreacted Li_3PO_4 (Figure 1d), and this Li_3PO_4 phase can still be detected after 1 and 2 h (Figure 1e,f). After being solvothermally treated at 180 °C for 3 h, a phase-pure LFP was obtained, and the XRD pattern shows that all the peaks can be indexed to orthorhombic LFP (JCPDS No. 83-2092) (Figure 1g). The clear phase transformation from Li_3PO_4 to LFP without formation of any other intermediate products indicates a direct ion exchange reaction between Li_3PO_4 and Fe^{2+} ions at 180 °C in EG medium.

The SEM image shows that the phase-pure LFP product exhibits good morphology maintenance and a similar size distribution of ~1 μm with Li_3PO_4 (Figure 2d). The TEM image shows that the LFP microspheres also have a hollow structure (Figure 2e). However, the magnified TEM image shows that the hollow part and the shell of LFP become smaller and thicker than that of Li_3PO_4, respectively (Figure 2f). A proper explanation is that the shell of Li_3PO_4 has been expended due to the substitution of Fe^{2+} for Li^+.

3.2. Influences of the Solvent and Iron Source on the Products. The successful synthesis of phase-pure LFP with good shape and structure maintenance is strongly dependent on the medium and iron source. Under identical reaction conditions, when H_2O was used as the medium, an impurity of $Fe_3(PO_4)_2(OH)_2$ (JCPDS No. 36-0045) was formed (Figure S1a, Supporting Information), and broken spheres with irregular particles were obtained in the final product (Figure S2a, Supporting Information). The reason may be attributed to the dissolution−precipitation reaction between Li_3PO_4 templates and Fe^{2+} ions in H_2O, which is similar to the reported process,[65] leading to breakage of the Li_3PO_4 templates and formation of impurity in the final product. On the other hand, when the $FeSO_4{\cdot}7H_2O$ was used as the iron source while keeping other parameters constant, the ion exchange reaction between Li_3PO_4 templates and Fe^{2+} ions was hindered and some unknown impurity was also formed in the final product (Figure S1b, Supporting Information). The SEM image shows that the spherical morphology of the templates can be maintained but some quadrangular-like shell appeared (Figure S2b, Supporting Information); this unknown product may be responsible for the impurity phase in the final product.

Actually, a white material which can be removed by water-washing was observed when the Teflon container was opened. In order to understand what the material is, the product was washed by EG and ethanol, respectively. The SEM image and XRD pattern show that the white material has a huge quadrangular-like shape and can be indexed to $FeSO_4{\cdot}H_2O$ (Figure S3a,b, Supporting Information). We believe that the dehydration process of $FeSO_4{\cdot}7H_2O$ under the solvothermal condition resulted in the recrystallization of the insoluble $FeSO_4{\cdot}H_2O$ in EG, blocking the reaction between Fe^{2+} and Li_3PO_4 micro hollow spheres, because the $FeSO_4{\cdot}7H_2O$ is soluble in EG solvent; it can dehydrate into $FeSO_4{\cdot}H_2O$ when the temperature is higher than 100 °C, and the $FeSO_4{\cdot}H_2O$ is stable until 240 °C (Figure S3c, Supporting Information). Furthermore, there must be some unknown reactions around the surface of this quadrangular-like $FeSO_4{\cdot}H_2O$ crystal, causing an insoluble impurity in water; this can explain why there are some quadrangular-like shells existing in the final product after water-washing (Figure S2b, Supporting Information).

3.3. Reaction Mechanism. Scheme 1 shows a proper mechanism of the ion exchange reaction between the Li_3PO_4 templates and Fe^{2+} ions in EG medium. The successful transformation from Li_3PO_4 to LFP with good morphology maintenance can ascribe to (i) Li_3PO_4 and LFP belonging to the same orthorhombic system, leading to easier structure transformation; (ii) the interface between the aggregated Li_3PO_4 nanoparticles enabling the move of Fe^{2+} ions into the inside of the Li_3PO_4 micro hollow spheres under solvothermal condition. At room temperature, the Fe^{2+} ions could only adsorb onto the surface of the Li_3PO_4 micro hollow spheres without reaction, while under solvothermal condition, the higher temperature and the reaction between Fe^{2+} ions and Li_3PO_4 nanoparticles provide a motive power for the diffusion of Fe^{2+} ions into the inside of the Li_3PO_4 micro hollow spheres. (iii) The most important reason is that the aggregated Li_3PO_4 nanoparticles have a short path for the penetration of Fe^{2+} ions into the Li_3PO_4 nanocrystal, leading to a fast and complete ion exchange reaction without kinetic block. We believe that the

Scheme 1. Illustration of the Ion Exchange Reaction between Single Li_3PO_4 Micro Hollow Sphere and Fe^{2+} Ions

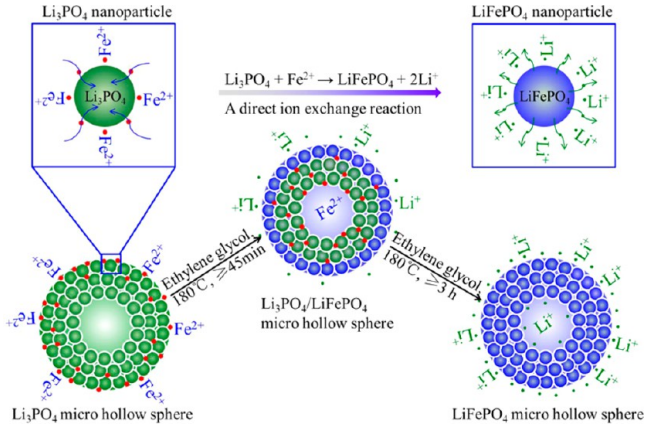

ion exchange reaction between Li_3PO_4 nanoparticles and Fe^{2+} ions is direct and fast, but the reaction between a single Li_3PO_4 micro hollow sphere and Fe^{2+} ions should start from the surface to inside of the hollow sphere step by step, and the reaction can be achieved within 2 h at 180 °C according to the XRD patterns.

3.4. Carbon Coated LFP and Its Electrochemical Performances. The carbon coated LFP micro hollow spheres were achieved by a glucose solution impregnating−drying−sintering procedure, which is similar to the reported process to carbon coat the mesoporous LFP microspheres.[60] Figure 3a shows the TEM image of one single carbon coated LFP micro hollow spheres, which still exhibits good spherical shape; the formation of detached particles on the surface should be caused by the external force of the magnetic stirring. The HRTEM image of the LFP nanoparticles on the surface of the carbon coated LFP micro hollow spheres shows that the LFP nanoparticle exhibited beautiful crystal lattices and could be coated with a uniform carbon layer of ~3.5 nm (Figure 3b). After the impregnating and drying process, the LFP microspheres should be coated with a uniform glucose layer because of the adsorption of the glucose molecules onto the surface of LFP microspheres. In the subsequent sintering procedure, the glucose molecules could melt to liquid state, and the interfaces between the LFP nanoparticles expanded due to the shrink of LFP nanoparticles along with the increase of temperature; all these state changes and high temperature are beneficial to the diffusion of glucose and carbon coating of the inner nanoparticles of the LFP microspheres.

The carbon content in the carbon coated LFP microspheres was estimated by thermogravimetric (TG) measurement of the carbon free and the carbon coated LFP products in oxygen atmosphere (Figure 4). According to the previous report,[60,67]

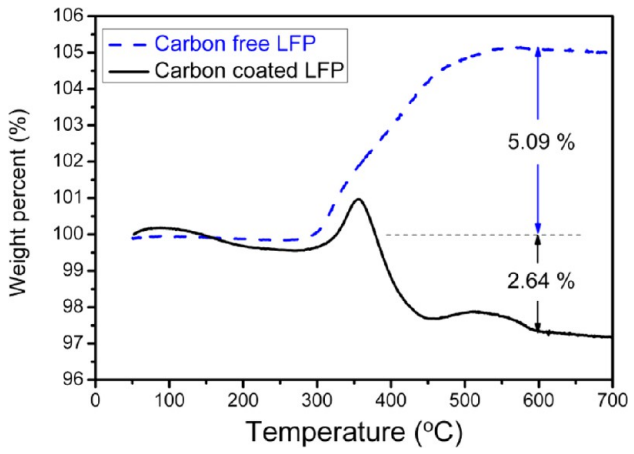

Figure 4. TG curves of the carbon free and carbon coated LFP microspheres recorded with a heating rate of 10 °C min^{-1} in an oxygen atmosphere.

the carbon free LFP can be oxidized to $Li_3Fe_2(PO_4)_3$ and Fe_2O_3 with a theoretical weight gain of 5.07 %, while the carbon coated LFP can also be oxidized to these two products and CO_2 gas with different weight change (influenced by the amount of carbon content). In our case, the carbon free and carbon coated LFP could gain 5.09 % and lose 2.64 % of the total weight, respectively. By neglecting the tiny deviation, the carbon content of the carbon coated LFP microspheres was estimated as ~7.7 wt % (5.09 % + 2.64 %).

The rate performances were estimated under a galvanostatic charge−discharge mode with same the C-rates. Figure 5a shows that the carbon coated LFP micro hollow spheres can exhibit a superior rate performance, capacities as high as 158, 144, 125, 101, and even 72 mAh g^{-1} could be obtained at 0.1, 1, 5, 20, and 50 C, respectively. Figure 5b shows the cycling performance of the carbon coated LFP micro hollow spheres, which was recorded after the rate performance. The electrode was charged−discharged at 0.5 C for 3 times, 20 C for 2000 times,

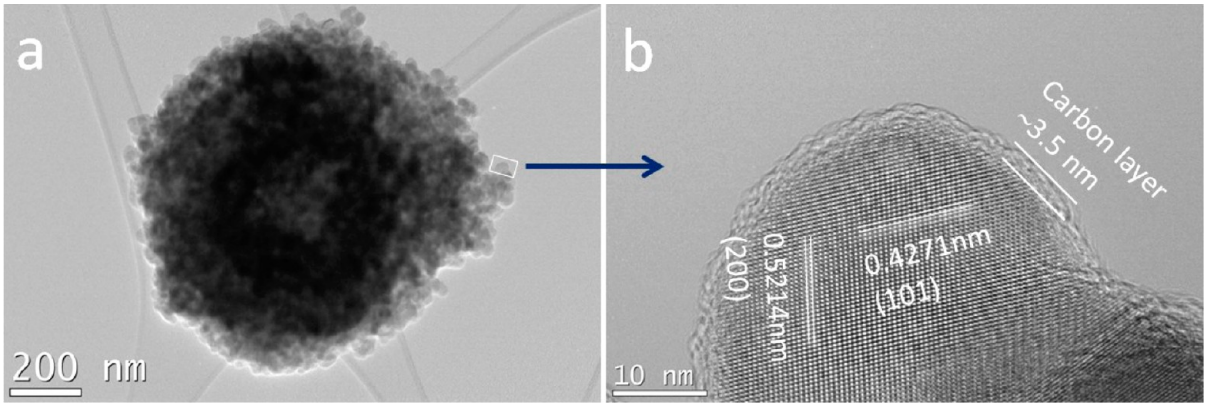

Figure 3. (a) Overview TEM image of one single carbon coated LFP micro hollow sphere; (b) HRTEM image of the LFP nanoparticles on the surface of the carbon coated LFP micro hollow spheres.

dx.doi.org/10.1021/am401990b | ACS Appl. Mater. Interfaces 2013, 5, 8961−8967

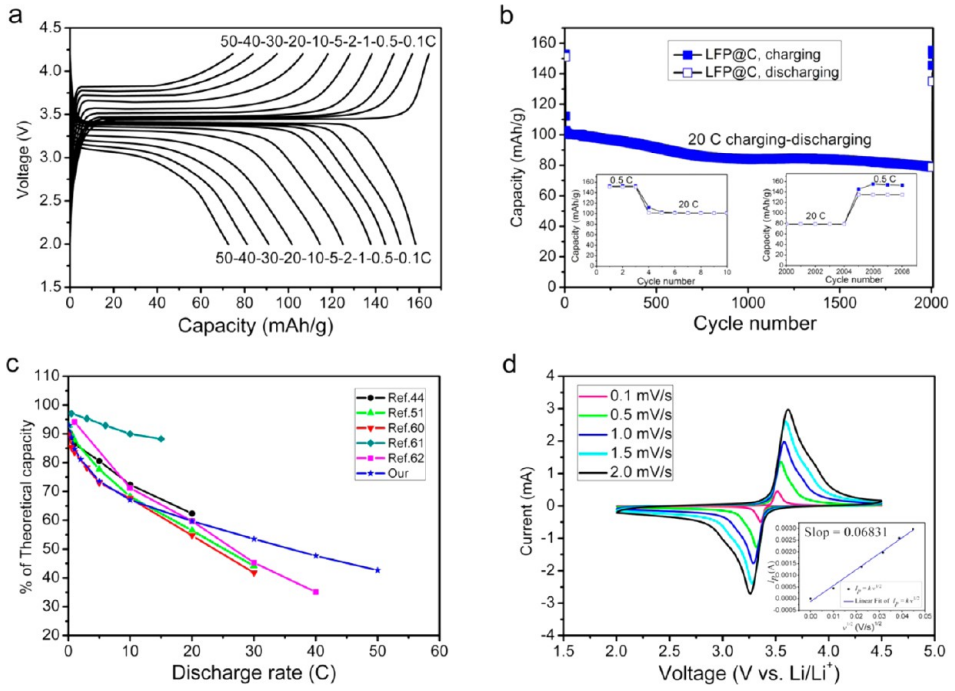

Figure 5. (a) Rate performances and (b) cycling performance of the carbon coated LFP micro hollow spheres, (c) comparison of the rate capacity retention of our carbon coated LFP micro hollow spheres with those best results of the spherical LFP materials synthesized by various methods, and (d) CV curves for carbon coated LFP micro hollow spheres at scan rates from 0.1 to 2 mV s^{-1}.

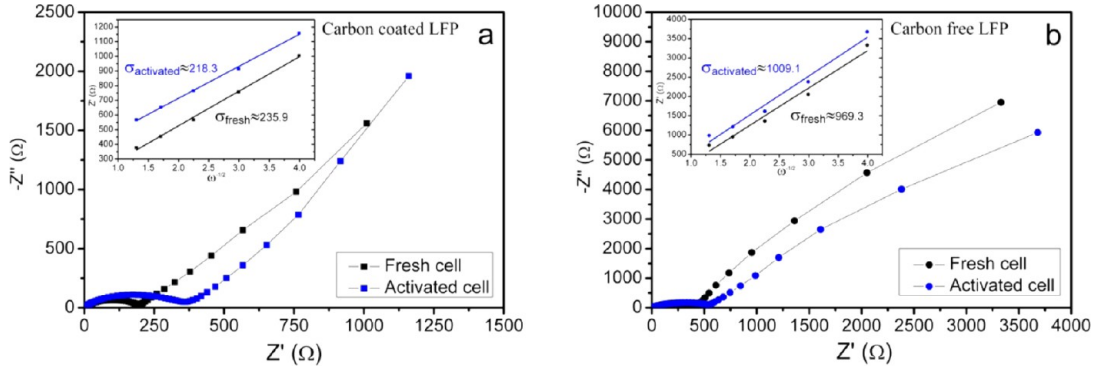

Figure 6. Nyquist plots (Z' vs. $-Z''$) of (a) carbon coated LFP microspheres and (b) carbon free LFP microspheres. Insets are the relationship plots of Z' vs. $\omega^{-1/2}$ at low-frequency region. The open circuit voltage (OCV) of the fresh cell is 2.5 and 2.8 V for carbon coated and carbon free LFP microspheres, respectively. The activated cells are fully charged−discharged at a 0.1 C rate for two times.

and then recycled at 0.5 C for 3 times. As can be seen, the electrode can deliver reversible charge−discharge capacity of 152−151 mAh g^{-1} at 0.5 C, and it can still maintain 80% of the initial discharge capacity of 101 mAh g^{-1} after cycling for 2000 times at 20 C. When it was recycled at 0.5 C, the electrode showed a similar charge capacity of 152 mAh g^{-1} but a lower discharge capacity of 135 mAh g^{-1} compared with the initial values at 0.5 C, indicating a fading of the discharge capacity of the electrode after high rate cycling. Figure 5c shows the comparison of the rate capacity retention of our carbon coated LFP micro hollow spheres with those best results of the spherical LFP materials synthesized by various methods. Except the best results reported by Lim et al. (Ref 61), our carbon coated LFP micro hollow spheres were found to exhibit higher capability retention than others at high rate over 20 C. However, it is worth noticing that the LFP micro hollow spheres have a low tap density of ~0.9 g cm^{-3}; the low tap density will consume the energy density of the product. In order to increase the tap density of the LFP microspheres, synthesis of a solid, polycrystal, microspherical Li_3PO_4 template is favorable.

Figure 5d shows the cyclic voltammerty (CV) curves of the carbon coated LFP micro hollow spheres recorded at different scan rates after "activation" at a scan rate of 0.1 mV s^{-1}. The Randles-Sevcik equation[68] was used to calculate the Li-ion diffusion coefficient D (cm^2 s^{-1}):

$$I_p = 2.69 \times 10^5 A \cdot C \cdot D^{1/2} \cdot n^{3/2} \cdot v^{1/2} \quad (1)$$

where I_p is the peak currents (Amperes), A is the electrode area (cm^2), C is the shuttle concentration (mol cm^{-3}, derived from the theoretical mass density of LFP, 3.6 g cm^{-3}), n is the number of electrons involved in the redox process (n = 1 for Fe^{2+}/Fe^{3+} redox pair), and v is the scan rate (V s^{-1}). Lines through the zero point could be fitted (inset in Figure 5d), and a slope value of 0.06831 was obtained; the Li-ion diffusion coefficients of the carbon coated LFP micro hollow spheres

dx.doi.org/10.1021/am401990b | ACS Appl. Mater. Interfaces 2013, 5, 8961−8967

were calculated as 3.96×10^{-11} cm^2 s^{-1}, which is three orders of magnitude higher than the reported value of $\sim 10^{-14}$ cm^2 s^{-1}.[69]

Electrochemical impedance spectroscopy (EIS) examination was also carried out to clarify the difference in the electrochemical response of the fresh cells and activated cells assembled with carbon free or carbon coated LFP electrodes (Figure 6). According to the follow equation:[70]

$$Z' = R_s + R_{ct} + \sigma\omega^{-1/2} \quad (2)$$

where R_s is the resistance of solid polymer electrolytes; an intercept at the Z' axis in a high frequency region can correspond to R_s, whose value is usually small and similar; R_{ct} is the charge transfer resistance, the combination of one compressed semicircle in the high-to-medium frequency range on the Z' axis is approximately equal to R_{ct}; σ is the Warburg factor, which is associated with lithium-ion diffusion; and ω is the angular frequency ($\omega = 2\pi f$); the inclined line in the low frequency region represents the Warburg impedance ($\sigma\omega^{-1/2}$). It can be seen that the carbon coated LFP electrodes have smaller resistance than the carbon free LFP electrodes. From view of the R_{ct}, both R_{ct} of these two kinds of LFP electrodes increased after the charge−discharge at 0.1 C rate for two times; this may be caused by the disorder of the charges in the activated cells. From view of Warburg impedance, however, the electrochemical response of the fresh cells and the activated cells are different among these two kinds of LFP electrodes. Four Warburg factors were derived from the linear fit of the last five dots in the low frequency regions (insets in the Figure 6). As it can be seen, the σ decreased for carbon coated LFP and increased for the carbon free LFP after being activated at 0.1 C. According to the reciprocal relationship of the lithium ion diffusion (D) and σ^{-2} ($D \propto 1/\sigma^{-2}$),[70] lithium ion diffusion will increase along with the decrease of σ. The reason why the lithium ion diffusion increases for carbon coated LFP electrode and decreases for carbon free LFP electrode after activation of the fresh cells is not clear. It was said that the solid electrolyte interface (SEI) allows facile Li-ion migration through them between the solution and graphite phase.[71] Did the carbon layer on the LFP nanoparticles also promote the formation of SEI that is usually formed at the surface of the carbon negative electrode?

4. CONCLUSIONS

In summary, monodisperse, Li_3PO_4 micro hollow spheres composed of tiny nanoparticles could be easily transformed into polycrystal LFP micro hollow spheres. The solvothermal reaction between Li_3PO_4 and Fe^{2+} ions in EG medium was finely explained by a direct ion exchange reaction. In order to obtain a phase-pure LFP with good morphology retention, H_2O and ferrous sulfates should be restricted in the reaction system, because they could make the reaction more complicated. The carbon coted LFP micro hollow spheres could exhibit higher lithium ion diffusion coefficient and superior rate and cycling performances. Compared with the hard template routes, this self-sacrificed template method is simple and fast. It may provide an effective strategy to access other polycrystal $LiMPO_4$ micro hollow spheres (M = Mn, Co, or Ni).

■ ASSOCIATED CONTENT

Supporting Information

The influences of the iron source and solvent on the phase and morphology of the products, investigated by XRD, SEM, and TGA. This information is available free of charge via the Internet at http://pubs.acs.org/.

■ AUTHOR INFORMATION

Corresponding Author

*E-mail: appchung@cityu.edu.hk. Tel.: (+852) 34427835. Fax: (+852) 34420538.

Author Contributions

Y.-C. Dong was added as the author because of his help on the HRTEM characterization of the carbon coated LFP.

Notes

The authors declare no competing financial interest.

■ ACKNOWLEDGMENTS

J. C. Y. Chung is thankful for the financial support from the GRF Grant (#9041528, CityU 100510) from the Hong Kong SAR government Research Grant Council.

■ REFERENCES

(1) Armand, M.; Tarascon, J. M. *Nature* **2008**, *451*, 652−657.
(2) Kang, B.; Ceder, G. *Nature* **2009**, *458*, 190−193.
(3) Arico, A. S.; Bruce, P.; Scrosati, B.; Tarascon, J. M.; Van Schalkwijk, W. *Nat. Mater.* **2005**, *4*, 366−377.
(4) Dunn, B.; Kamath, H.; Tarascon, J. M. *Science* **2011**, *334* (6058), 928−935.
(5) Padhi, A. K.; Nanjundaswamy, K. S.; Goodenough, J. B. *J. Electrochem. Soc.* **1997**, *144*, 1188−1194.
(6) Chung, S. Y.; Bloking, J. T.; Chiang, Y. M. *Nat. Mater.* **2002**, *1*, 123−128.
(7) Delacourt, C.; Poizot, P.; Tarascon, J. M.; Masquelier, C. *Nat. Mater.* **2005**, *4*, 254−260.
(8) Delmas, C.; Maccario, M.; Croguennec, L.; Le Cras, F.; Weill, F. *Nat. Mater.* **2008**, *7*, 665−671.
(9) Ellis, B. L.; Makahnouk, W. R. M.; Makimura, Y.; Toghill, K.; Nazar, L. F. *Nat. Mater.* **2007**, *6*, 749−753.
(10) Gibot, P.; Casas-Cabanas, M.; Laffont, L.; Levasseur, S.; Carlach, P.; Hamelet, S.; Tarascon, J. M.; Masquelier, C. *Nat. Mater.* **2008**, *7*, 741−747.
(11) Herle, P. S.; Ellis, B.; Coombs, N.; Nazar, L. F. *Nat. Mater.* **2004**, *3*, 147−152.
(12) Nishimura, S.; Kobayashi, G.; Ohoyama, K.; Kanno, R.; Yashima, M.; Yamada, A. *Nat. Mater.* **2008**, *7*, 707−711.
(13) Yamada, A.; Koizumi, H.; Nishimura, S. I.; Sonoyama, N.; Kanno, R.; Yonemura, M.; Nakamura, T.; Kobayashi, Y. *Nat. Mater.* **2006**, *5*, 357−360.
(14) Malik, R.; Zhou, F.; Ceder, G. *Nat. Mater.* **2011**, *10*, 587−590.
(15) Tarascon, J. M.; Armand, M. *Nature* **2001**, *414*, 359−367.
(16) Goodenough, J. B.; Kim, Y. *Chem. Mater.* **2010**, *22*, 587−603.
(17) Islam, M. S.; Driscoll, D. J.; Fisher, C. A. J.; Slater, P. R. *Chem. Mater.* **2005**, *17*, 5085−5092.
(18) Zaghib, K.; Mauger, A.; Goodenough, J. B.; Gendron, F.; Julien, C. M. *Chem. Mater.* **2007**, *19*, 3740−3747.
(19) Wang, C. S.; Hong, J. *Electrochem. Solid State Lett.* **2007**, *10*, A65−A69.
(20) Kim, D. H.; Kim, J. *Electrochem. Solid State Lett.* **2006**, *9*, A439−A442.
(21) Wang, Y. G.; Wang, Y. R.; Hosono, E. J.; Wang, K. X.; Zhou, H. S. *Angew. Chem., Int. Ed.* **2008**, *47*, 7461−7465.
(22) Wu, X. L.; Jiang, L. Y.; Cao, F. F.; Guo, Y. G.; Wan, L. J. *Adv. Mater.* **2009**, *21*, 2710−2714.
(23) Hu, Y. S.; Guo, Y. G.; Dominko, R.; Gaberscek, M.; Jamnik, J.; Maier, J. *Adv. Mater.* **2007**, *19*, 1963−1966.

(24) Huang, Y. H.; Goodenough, J. B. *Chem. Mater.* **2008**, *20*, 7237−7241.
(25) Lepage, D.; Michot, C.; Liang, G. X.; Gauthier, M.; Schougaard, S. B. *Angew. Chem., Int. Ed.* **2011**, *50*, 6884−6887.
(26) Zhu, C. B.; Yu, Y.; Gu, L.; Weichert, K.; Maier, J. *Angew. Chem., Int. Ed.* **2011**, *50*, 6278−6282.
(27) Oh, S. W.; Huang, Z. D.; Zhang, B. A.; Yu, Y.; He, Y. B.; Kim, J. K. *J. Mater. Chem.* **2012**, *22*, 17215−17221.
(28) Zhang, L. L.; Liang, G.; Ignatov, A.; Croft, M. C.; Xiong, X. Q.; Hung, I. M.; Huang, Y. H.; Hu, X. L.; Zhang, W. X.; Peng, Y. L. *J. Phys. Chem. C* **2011**, *115*, 13520−13527.
(29) Zhang, X. G.; Zhang, X. D.; He, W.; Yue, Y. Z.; Liu, H.; Ma, J. Y. *Chem. Commun.* **2012**, *48*, 10093−10095.
(30) Shi, Y.; Chou, S. L.; Wang, J. Z.; Wexler, D.; Li, H. J.; Liu, H. K.; Wu, Y. P. *J. Mater. Chem.* **2012**, *22*, 16465−16470.
(31) Lee, K. S.; Myung, S. T.; Sun, Y. K. *Chem. Mater.* **2007**, *19*, 2727−2729.
(32) Sun, Y. K.; Oh, S. M.; Park, H. K.; Scrosati, B. *Adv. Mater.* **2011**, *23*, 5050−5054.
(33) Amine, K.; Belharouak, I.; Chen, Z. H.; Tran, T.; Yumoto, H.; Ota, N.; Myung, S. T.; Sun, Y. K. *Adv. Mater.* **2010**, *22*, 3052−3057.
(34) Shen, L. F.; Yuan, C. Z.; Luo, H. J.; Zhang, X. G.; Xu, K.; Xia, Y. Y. *J. Mater. Chem.* **2010**, *20*, 6998−7004.
(35) Du, X. Y.; He, W.; Zhang, X. D.; Yue, Y. Z.; Liu, H.; Zhang, X. G.; Min, D. D.; Ge, X. X.; Du, Y. *J. Mater. Chem.* **2012**, *22*, 5960−5969.
(36) Liu, H. S.; Bi, Z. H.; Sun, X. G.; Unocic, R. R.; Paranthaman, M. P.; Dai, S.; Brown, G. M. *Adv. Mater.* **2011**, *23*, 3450−3454.
(37) Zhou, L.; Zhao, D. Y.; Lou, X. W. *Angew. Chem., Int. Ed.* **2012**, *51*, 239−241.
(38) Liu, J.; Zhou, Y. C.; Wang, J. B.; Pan, Y.; Xue, D. F. *Chem. Commun.* **2011**, *47*, 10380−10382.
(39) Lai, X. Y.; Halpert, J. E.; Wang, D. *Energy Environ. Sci.* **2012**, *5*, 5604−5618.
(40) Yu, F.; Zhang, J. J.; Yang, Y. F.; Song, G. Z. *J. Mater. Chem.* **2009**, *19*, 9121−9125.
(41) Yu, F.; Zhang, J. J.; Yang, Y. F.; Song, G. Z. *J. Power Sources* **2009**, *189*, 794−797.
(42) Huang, B.; Zheng, X. D.; Jia, D. M.; Lu, M. *Electrochim. Acta* **2010**, *55*, 1227−1231.
(43) Yu, F.; Zhang, J. J.; Yang, Y. F.; Song, G. Z. *J. Power Sources* **2010**, *195*, 6873−6878.
(44) Liu, J.; Conry, T. E.; Song, X. Y.; Doeff, M. M.; Richardson, T. J. *Energy Environ. Sci.* **2011**, *4*, 885−888.
(45) Oh, S. W.; Myung, S. T.; Bang, H. J.; Yoon, C. S.; Amine, K.; Sun, Y. K. *Electrochem. Solid State Lett.* **2009**, *12*, A181−A185.
(46) Oh, S. W.; Myung, S. T.; Oh, S. M.; Oh, K. H.; Amine, K.; Scrosati, B.; Sun, Y. K. *Adv. Mater.* **2010**, *22*, 4842−4845.
(47) Wu, Y. M.; Wen, Z. H.; Li, J. H. *Adv. Mater.* **2011**, *23*, 1126−1129.
(48) Xie, H. M.; Wang, R. S.; Ying, J. R.; Zhang, L. Y.; Jalbout, A. F.; Yu, H. Y.; Yang, G. L.; Pan, X. M.; Su, Z. M. *Adv. Mater.* **2006**, *18*, 2609−2613.
(49) Oh, S. M.; Myung, S. T.; Park, J. B.; Scrosati, B.; Amine, K.; Sun, Y. K. *Angew. Chem., Int. Ed.* **2012**, *51*, 1853−1856.
(50) Oh, S. M.; Myung, S. T.; Choi, Y. S.; Oh, K. H.; Sun, Y. K. *J. Mater. Chem.* **2011**, *21*, 19368−19374.
(51) Lou, X. M.; Zhang, Y. X. *J. Mater. Chem.* **2011**, *21*, 4156−4160.
(52) Park, Y.; Shin, W.; Lee, J. W. *CrystEngComm* **2012**, *14*, 4612−4617.
(53) Zhang, C. J.; He, X.; Kong, Q. S.; Li, H.; Hu, H.; Wang, H. B.; Gu, L.; Wang, L.; Cui, G. L.; Chen, L. Q. *CrystEngComm* **2012**, *14*, 4344−4349.
(54) Su, J.; Wu, X. L.; Yang, C. P.; Lee, J. S.; Kim, J.; Guo, Y. G. *J. Phys. Chem. C* **2012**, *116*, 5019−5024.
(55) Deng, H. G.; Jin, S. L.; Zhan, L.; Wang, Y. L.; Qiao, W. M.; Ling, L. C. *J. Power Sources* **2012**, *220*, 342−347.
(56) Sun, C. W.; Rajasekhara, S.; Goodenough, J. B.; Zhou, F. *J. Am. Chem. Soc.* **2011**, *133*, 2132−2135.
(57) Shu, H. B.; Wang, X. Y.; Wu, Q.; Ju, B. W.; Liu, L.; Yang, X. K.; Wang, Y. P.; Bai, Y. S.; Yang, S. Y. *J. Electrochem. Soc.* **2011**, *158*, A1448−A1454.
(58) Wei, W.; Chen, D. Z.; Wang, R. N.; Guo, L. *Nanotechnology* **2012**, *23*, 475401.
(59) Popovic, J.; Demir-Cakan, R.; Tornow, J.; Morcrette, M.; Su, D. S.; Schlogl, R.; Antonietti, M.; Titirici, M. M. *Small* **2011**, *7*, 1127−1135.
(60) Qian, J. F.; Zhou, M.; Cao, Y. L.; Ai, X. P.; Yang, H. X. *J. Phys. Chem. C* **2010**, *114*, 3477−3482.
(61) Lim, S. Y.; Yoon, C. S.; Cho, J. P. *Chem. Mater.* **2008**, *20*, 4560−4564.
(62) Huang, Z. D.; Oh, S. W.; He, Y. B.; Zhang, B.; Yang, Y.; Mai, Y. W.; Kim, J. K. *J. Mater. Chem.* **2012**, *22*, 19643−19645.
(63) Lee, M. H.; Kim, J. Y.; Song, H. K. *Chem. Commun.* **2010**, *46*, 6795−6797.
(64) Lee, M. H.; Kim, T. H.; Kim, Y. S.; Park, J. S.; Song, H. K. *J. Mater. Chem.* **2012**, *22*, 8228−8234.
(65) Lee, M. H.; Kim, T. H.; Kim, Y. S.; Song, H. K. *J. Phys. Chem. C* **2011**, *115*, 12255−12259.
(66) Yang, S. L.; Ma, R. G.; Hu, M. J.; Xi, L. J.; Lu, Z. G.; Chung, C. Y. *J. Mater. Chem.* **2012**, *22*, 25402−25408.
(67) Belharouak, I.; Johnson, C.; Amine, K. *Electrochem. Commun.* **2005**, *7*, 983−988.
(68) Cho, Y. D.; Fey, G. T. K.; Kao, H. M. *J. Power Sources* **2009**, *189*, 256−262.
(69) Yu, D. Y. W.; Fietzek, C.; Weydanz, W.; Donoue, K.; Inoue, T.; Kurokawa, H.; Fujitani, S. *J. Electrochem. Soc.* **2007**, *154*, A253−A257.
(70) Jin, B.; Jin, E. M.; Park, K. H.; Gu, H. B. *Electrochem. Commun.* **2008**, *10*, 1537−1540.
(71) Aurbach, D.; Teller, H.; Levi, E. *J. Electrochem. Soc.* **2002**, *149*, A1255−A1266.